Research Collection School Of Computing and Information Systems

School of Computing and Information Systems

Dynamic-MUSIC: Accurate device-free indoor localization

Xiang LI
Peking University

Shengjie LI
Peking University

Daqing ZHANG
Peking University

Jie XIONG
Singapore Management University, jxiong@smu.edu.sg

Yasha WANG
Peking University

See next page for additional authors

Follow this and additional works at: https://ink.library.smu.edu.sg/sis_research

Part of the Software Engineering Commons

Author

Xiang LI, Shengjie LI, Daqing ZHANG, Jie XIONG, Yasha WANG, and Hong MEI

Dynamic-MUSIC: Accurate Device-Free Indoor Localization

Xiang Li[1,2], **Shengjie Li**[1,2], **Daqing Zhang**[1,2], **Jie Xiong**[4], **Yasha Wang**[1,3], **Hong Mei**[1,2]

[1]Key Laboratory of High Confidence Software Technologies, Ministry of Education, Beijing, China
[2]School of Electronics Engineering and Computer Science, Peking University, China
[3]National Engineering Research Center of Software Engineering, Peking University, China
[4]School of Information Systems, Singapore Management University, Singapore
{lixiang13,lishengjie,dqzsei,wangyasha,meih}@pku.edu.cn;jxiong@smu.edu.sg

ABSTRACT

Device-free passive indoor localization is playing a critical role in many applications such as elderly care, intrusion detection, smart home, etc. However, existing device-free localization systems either suffer from labor-intensive offline training or require dedicated special-purpose devices. To address the challenges, we present our system named MaTrack, which is implemented on commodity off-the-shelf Intel 5300 Wi-Fi cards. MaTrack proposes a novel Dynamic-MUSIC method to detect the subtle reflection signals from human body and further differentiate them from those reflected signals from static objects (furniture, walls, etc.) to identify the human target's angle for localization. MaTrack does not require any offline training compared to existing signature-based systems and is insensitive to changes in environment. With just two receivers, MaTrack is able to achieve a median localization accuracy below 0.6 m when the human is walking, outperforming the state-of-the-art schemes.

ACM Classification Keywords

C.3 Special-purpose and application-based systems: Signal processing systems

Author Keywords

Indoor localization; Device-free; Angle-of-arrival.

INTRODUCTION

Indoor localization system is playing a more important role in many emerging applications, such as indoor navigation, augmented reality, disaster rescue, elderly care, etc. In recent years, Wi-Fi-based localization systems [2, 47, 51, 53] are considered most promising due to the ubiquitousness of Wi-Fi deployments in public, enterprises, universities and also homes. Earlier pioneering work [2] employs Received Signal Strength Indicator (RSSI) information widely available at the access points (APs) as a unique signature to locate the targets. Recently, with the adoption of MIMO technologies in the latest 802.11n and 802.11ac Wi-Fi standards, channel state

information (CSI) is employed for localization purposes [31, 47, 51]. Compared with coarse RSSI with only amplitude for the whole channel, CSI contains both amplitude and phase of each subcarrier, which has also been used for activity recognition [12, 35, 39, 54]. Another interesting trend with MIMO is more antennas are equipped at the latest 802.11n and 802.11ac APs. This unique opportunity enables angle-of-arrival (AoA) based localization systems [19, 47] which are able to achieve below 1 m accuracy. However, these systems still require the user to carry a device which could transmit or receive Wi-Fi signals. On the other hand, device-based localization is not applicable in a lot of scenarios. In elderly care, the elders are usually reluctant [34] to carry mobile or wearable devices. In intruder detection and terrorist tracking, the targets will deliberately discard any device that can be tracked. These real-life scenarios motivate the needs for device-free localization in recent years.

The state-of-the-art device-free approaches on commodity Wi-Fi devices employ RSSI or CSI as fingerprints [1, 30, 53], which need substantial radio-map survey and labor-intensive offline training. Once there are changes in the monitoring environment, the fingerprint database needs to be updated accordingly which is time consuming. Furthermore, the performance of fingerprint-based methods decreases significantly when the target is moving. The Doppler shifts due to target movements make the signature-location relationship unstable so a high localization accuracy is difficult to be achieved. Existing solutions either require high density deployment [22, 42] or need dedicated devices to send out customized signals [18, 42], limiting large scale deployments in real life. To the best of our knowledge, an accurate device-free localization system hosted on commodity Wi-Fi infrastructure for a mobile target is still missing.

Recently, the multiple signal classification (MUSIC) algorithm [29] is widely employed to estimate the AoA of incoming signals for device-based localization [19, 47] as shown in Figure 1(a). One key challenge for AoA-based systems is the strong multipath reflections in an indoor environment and only the direct path is pointing to the true location of the target. However, for device-free localization, the direct path is not related to the location of the target. As shown in Figure 1(b), different from device-based localization, the reflection path now contains the angle information of the target to the receiver. The target serves like a relay transmitter to reflect the signal to the receiver. If there are more than one Wi-Fi receivers and
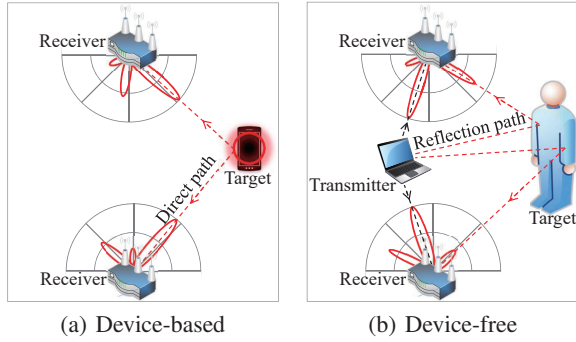
| (a) Device-based | (b) Device-free |

Figure 1. AoA-based localization

each could obtain the target's AoA from the reflection path, we can locate the target with triangulation.

In this paper, we propose a device-free passive indoor localization system called MaTrack using commodity Wi-Fi chipsets without a need of radio-map survey or any hardware modification. To realize it as a functional system, a number of challenges need to be addressed:

- Different from device-based localization identifying the direct path, for device-free localization, the signal reflected from the target (human) is what we care about. In a typical indoor environment, there is only one direct path but multiple reflection paths from the target and other reflectors, such as walls and furniture. We need to identify which path is from the target for localization.

- Compared to direct path signal, reflection path signals are much weaker. With a 3-antenna AP, the traditional MUSIC algorithm is only able to capture a maximum of two signals including the direct path signal and the strongest multipath signal. The reflection signal from the target usually is not the strongest. Therefore, detecting a reflection path from the target with a limited number of antennas is challenging.

- The reflected signal from the target may be further reflected by other objects before reaching the receiver. If the target is not the last reflector, the signal does not contain the angle information of the target. We need to identify those reflection paths directly from the target without other reflections.

To address these challenges, we propose a novel Dynamic-MUSIC method to detect the weak signal reflected from the moving target and obtain the corresponding AoA for localization. The intuition is that, *signals reflected from the moving target keep changing and are incoherent with the direct path signal and signals only reflected by static objects. The direct path signal and signals only reflected by static objects are coherent with each other.* Coherency is considered harmful for the traditional MUSIC algorithm and different schemes [19, 32, 47] were proposed to remove the coherence among signals for accurate AoA estimation. Our Dynamic-MUSIC method, on the other hand, intelligently leverages this 'bad' coherence to merge the static signals and detect the signals reflected from the moving target. The paths reflected from the moving target are called *mobile paths* while the direct path and other reflection paths are called *static paths*. We employ the APs with

known locations to be the receivers and any Wi-Fi capable device can serve as the transmitter. The proposed method does not need to know the locations of transmitters. This property makes it flexible and can easily be adopted in different environments for large scale deployments. To summarize, we have made the following contributions in this paper:

1. We analyze the coherency relationship among signals in a multipath environment and prove that any mobile path signal is incoherent with static paths signals.

2. We propose a Dynamic-MUSIC method to identify the angle of the moving target. We intentionally keep the 'bad' coherence among signals to merge the static paths so the requirement of higher number of antennas is efficiently relaxed. By exploiting the stability of the paths, we are able to identify the mobile paths without any offline training. We leverage the relative ToA (time-of-arrival) information to identify the shortest mobile path to obtain the target's angle.

3. We propose a novel scheme to utilize the slight movement of the target to increase the detection rate and area coverage significantly. With only 2 receivers and 3 consecutive measurements within 0.04 s, the target can be detected close to 100% of the time. This sparse deployment property makes our method be an ideal candidate for large scale deployment.

4. We design and implement the system on Intel 5300 commodity Wi-Fi chipsets and evaluate the system in three indoor environments. With only 2 receivers, MaTrack is able to achieve a median localization accuracy of 52 cm and 62 cm when the target is spinning and walking, respectively.

The subsequent sections are organized as follows: Section 2 discusses the related work. In Section 3, we present the key intuitions of our method. Section 4 presents the detailed design. In Section 5, we evaluate our system in three real-life environments. We discuss the limitations related to our method in Section 6 followed by a conclusion in Section 7.

RELATED WORK
Different technologies have been employed for indoor localization, such as camera [3, 4], RF [2, 33, 36, 37, 50], infrared [8, 13], Ultra-wideband (UWB) [9], sound [14, 41], and recently visible light [15, 20], etc. While camera based system is able to achieve a high accuracy, good lightening condition and privacy concern are two big issues for real-life deployment. Sound based location systems are usually vulnerable to acoustic noise and the coverage area is limited. Dedicated infrastructures are needed for infrared base system while visible light only works in LoS scenarios. In this work, we focus on Wi-Fi based schemes as Wi-Fi APs are now widely deployed ubiquitously. Wi-Fi based indoor localization systems can be broadly categorized into two groups: device-based and device-free.

Device-based indoor localization with Wi-Fi
A lot of device-based systems have been proposed in literature. RADAR [2] is a pioneering system employing Wi-Fi RSSI information as a signature for localization and a lot of works are proposed later either to reduce the offline training load [5,

17] or improve the accuracy [49, 52]. In the last few years, fine-grained CSI was used for location estimation [31, 44, 51]. With 802.11n and 802.11ac standards, more antennas are equipped at a single AP and this opportunity is leveraged to obtain the AoA information for localization [19, 47]. However, all these works require the target to hold a device which could transmit Wi-Fi signals actively and the direct path signal is identified and used to locate the target.

While popular with UWB technology [9], time-based (ToA) localization is rare with Wi-Fi because the narrow channel bandwidth (20 - 40 MHz) is not enough to achieve a fine time resolution for indoor localization. With 802.11ac supporting a maximum of 160 MHz channel on 5 GHz band, some recent works [46, 48] propose to combine adjacent smaller channels to form a virtual larger channel to increase the resolution. However, the Wi-Fi channels on 5 GHz band are not continuous and non-adjacent channel combination is difficult. In 2.4 GHz band, a total of 70 MHz available bandwidth is still too narrow to achieve a high localization accuracy.

Device-free localization with Wi-Fi
In 2007, Youssef et al. [53] introduced the concept of device-free localization and a lot of works have been proposed since then. Seifeldin et al. developed the Nuzzer system [30] using the RSSI signature as a fingerprint. Pilot [45] and Mono-PHY [1] systems employ the finer CSI information as the fingerprint to improve the performance. E-eyes [40] utilizes the amplitude pattern of CSI to build a fingerprint map to identify the target's moving trajectory and accordingly determine the destination room. Ichnaea [28] is a device-free tracking system based on RSSI with an offline background training phase and is able to achieve a median accuracy of 2.5 m. All of these works need a substantial radio-map survey and labor-intensive fingerprint updates when there are changes in the environment. Ohara et al. [22] propose a fingerprint-based device-free method to locate the mobile target and apply model transformation scheme to reduce the offline training load. However, this method relies on the target's influence on the direct path signal. Thus, it needs a high density deployment to cover the monitoring area with an accuracy of around 2 m. Wilson et al. [42] introduce a radio tomographic imaging (RTI) method to achieve a high accuracy for moving target localization. This method also requires a dense deployment which is not realistic in most indoor environments. Different from these works, our MaTrack system utilizes the CSI subcarrier phase measurements across antennas to identify the moving target's angle information. MaTrack can locate the target passively with only two receivers and still achieves a high accuracy. Moreover, our scheme does not require any radio-map survey or offline training process and is robust against changes in the environment.

WiDeo [18] is a device-free system proposed to track the human's motion with Wi-Fi signals. WiDeo is implemented on the WARP software-defined radio platform [21] and hardware modification is required to implement it on commodity Wi-Fi cards. WiSee [23] is able to capture the Doppler shift introduced by a moving object for gesture recognition. The amount of Doppler shift is dependent on the object's moving
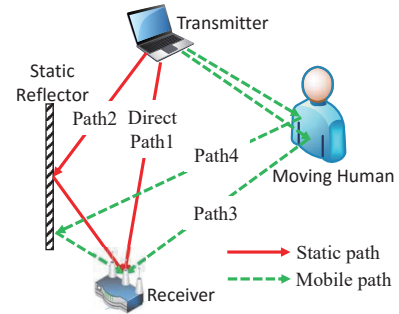

Figure 2. Multipath environment with a moving human

speed, which has also been used for sleep sensing [24] and facial gesture recognition [10]. However, all the above systems are built on dedicated special-purpose hardware. The Doppler shift introduced by a moving human is merely a few hertz while the frequency offset between the transmitter and receiver can be up to several hundreds hertz. This makes it challenging to detect the small Doppler shift for localization on commodity Wi-Fi cards. Furthermore, in order to obtain an accurate Doppler shift for localization, the packet interval needs to be measured in an accuracy level of nano-seconds which is very hard with commodity Wi-Fi cards.

The MIMO radar [16, 38, 55] uses phased array techniques to locate target in the outdoor environment. It requires a high number of antennas and dedicated FMCW signal to identify the target's accurate AoA and ToA information, while FMCW signal is not compatible with the Wi-Fi standards. Different from these works, our MaTrack system is implemented on the off-the-shelf commodity Wi-Fi chipsets with only 3 antennas without any hardware modification.

MULTIPATH ENVIRONMENT WITH A MOVING HUMAN
In a typical indoor environment, the Wi-Fi signal is propagated not only along the direct path, but also reflected by objects, walls, ceilings and floors. The signal received at the receiver is a superposition of signals from all the paths. Suppose the Wi-Fi signals arrive at the receiver through n different paths, including the direct path, we express the overall signal as:

$$\mathbf{S}(t) = [s_1(t), \dots, s_n(t)]^\top \quad (1)$$

where $s_i(t)$ represents the ith-path signal at time t.

Considering the scenario in Figure 2, where there are two reflectors (including the human target), the Wi-Fi signal is transmitted along the direct path and also reflected by the reflectors before arriving at the receiver. The human target may have more than one reflection paths to the receiver. When the target is moving, the reflection paths from the human target keep changing in terms of amplitude and phase. Before we introduce the detail design of MaTrack, we would like to present the following key insights of our method:

- **Static path signals are coherent with each other:** Static paths do not change with time. The shortest static path is the direct path and we express its signal as $s_{s,1}(t)$. The subscript s means it is a static path signal. The ith static path signal can be expressed as $s_{s,i}(t) = \alpha_i s_{s,1}(t)$, where α_i is a complex

number describing the gain and phase relationship between the ith static path and the direct path signals. All static path signals have the same central frequency and constant phase differences with each other. Thus, they are coherent.

- **Mobile path signals are incoherent with static path signals:** The movement of the human target will introduce a Doppler frequency shift on the signal. Besides the frequency, the lengths of mobile paths also keep changing. Similar to static paths, the jth mobile path signal can be expressed as $s_{m,j}(t) = \beta_j(t)s_{s,1}(t)$, where $\beta_j(t)$ is the complex number describing the gain and phase relationship between the jth mobile path signal and the direct static path signal at time t. Note $\beta_j(t)$ is not a constant value because the path length keeps changing when the target is moving. Because a mobile path signal goes through a round trip at the reflection surface, the path length change rate is approximately twice the radial velocity of the reflection surface [39]. Without loss of generality, we assume the radial velocity of the reflection surface is equal to the human target's moving speed. If the moving speed is 0.5 m/s, the phase change rate of the mobile path is $2\pi f v_{path}/c = 100$ $radians/s$ for a 5 GHz Wi-Fi signal. Therefore, the phase change is obvious and $\beta(t)$ is time variant. For two signals to be coherent with each other, they must have the same central frequency and a constant phase difference over time [43]. Therefore, mobile path signals are incoherent with static path signals.

- **Mobile path signals are incoherent with each other:** The human target can be treated as a polyhedron with multiple reflection surfaces. A human target may have more than one reflection paths from different reflection surfaces to the receiver. We observe that different reflection surfaces have different radial velocities so the phase change rates are also different. When the human is walking, the speed of the arms can be twice of the torso [7]. If the radial velocity difference is 0.1 m/s, the phase change rates have a difference of $2\pi f \Delta v_{path}/c = 20$ $radians/s$. Thus, mobile path signals are incoherent with each other.

According to the above three observations, we can rewrite Equation 1, the multipath signal vector, as:

$$\mathbf{S}(t) = [s_{s,1}(t), \ldots, s_{s,n_s}(t), s_{m,1}(t), \ldots, s_{m,n_m}(t)]^\top$$
$$= [\alpha_1 s_{s,1}(t), \ldots, \alpha_{n_s} s_{s,1}(t), s_{m,1}(t), \ldots, s_{m,n_m}(t)]^\top \quad (2)$$

where n_s and n_m are the numbers of static paths and mobile paths respectively.

- **The shortest mobile path contains the angle information of the target**: In an indoor environment, a reflection path may be reflected by more than one reflectors. For a mobile path, if the human target is the last reflector, the signal is like being 'transmitted' from the target and the AoA of this path can be employed to locate the target as the path 3 shown in Figure 2. If the human target is considered as a point, the mobile path only reflected by the human target is always the shortest mobile path. However, the human target has a non-negligible size and this statement is no longer true theoretically. In real life experiments, the path difference caused by the human size is much smaller compared to the
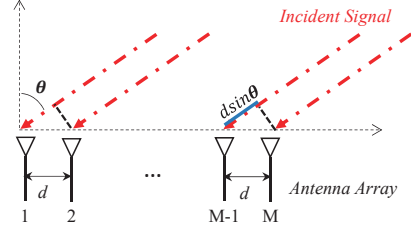

Figure 3. Antenna array with one incident signal

extra path distance caused by another reflector. Therefore, we are still able to treat the shortest mobile path as the one only reflected by the human target. The human target is the last reflector of the shortest mobile path, so its AoA can be employed to locate the target. We call the shortest mobile path *target path*.

DYNAMIC-MUSIC METHOD
In a typical indoor environment, there are around 4 - 8 significant reflection paths [6]. Besides the static paths from static reflectors, the moving target generates mobile paths. To locate the moving target, the key is to identify the target path and accurately estimate the AoA of this path. In the past few years, the well-known MUSIC algorithm [29] has been employed to estimate the direct path AoA for device-based localization. Different from previous work, we need to identify the AoA of the target path, which is a reflection path and is usually weak. There is only one direct path but usually many reflection paths. Thus, identifying the AoA of the weak target path is more challenging and the-state-of-art MUSIC-based methods can not be applied directly on commodity Wi-Fi devices to solve our problem. To address this challenge, we propose a novel Dynamic-MUSIC method to identify and accurately estimate the AoA of the target path. We first present the MUSIC algorithm followed by our method.

Estimating AoA with MUSIC
The basic idea of standard MUSIC algorithm is that incident signals from different angles introduce different amounts of phase changes on each antenna at the receiver. For clarity of explanation, we first introduce the phased array structure with only one incident signal and illustrate how to estimate the signal's AoA. Then we extend the model to handle multiple incident signals with MUSIC.

Phased array with one incident signal
Assume there is a linear array with M antennas at the receiver. An incident signal is received at the antenna array with an arriving angle θ, shown in Figure 3. The antenna spacing d is half-wavelength of the signal. The signal has different propagation lengths at different antennas. The propagation paths are much longer than the antenna spacing d, so the path difference between adjacent antennas can be expressed as $d \sin(\theta)$. Therefore, a phase difference of $-2\pi f d \sin(\theta)/c$ is introduced at adjacent antennas, where f is the signal frequency and c is the speed of light. We can thus denote the introduced phase difference as a function of the AoA:

$$\Phi(\theta) = e^{-j2\pi f d \sin(\theta)/c} \quad (3)$$

The phase differences at the antenna array are expressed as:

$$\mathbf{a}(\theta) = [1, \Phi(\theta), \ldots, \Phi(\theta)^{M-1}]^\top \qquad (4)$$

where $\mathbf{a}(\theta)$ is called the steering vector. If the signal received at the first antenna is $s(t)$, the received signal vector at the antenna array can be expressed as:

$$\mathbf{X}(t) = [x_1(t), \ldots, x_M(t)]^\top = \mathbf{a}(\theta)s(t) + \mathbf{N}(t) \qquad (5)$$

where $\mathbf{N}(t)$ is the noise vector. With only one incident signal, the AoA θ can be obtained easily by measuring the phase differences across antennas with Equation 3.

Phased array with multiple incident signals
When there are n incident signals arriving at the antenna array, the received signal at each antenna is the superposition of all incident signals. Based on Equation 5, the received signal vector is expressed as:

$$
\begin{aligned}
\mathbf{X}(t) &= [x_1(t), \ldots, x_M(t)]^\top \\
&= \sum_{i=1}^{n} \mathbf{a}(\theta_i)s_i(t) + \mathbf{N}(t) \\
&= \mathbf{AS}(t) + \mathbf{N}(t) \qquad (6)
\end{aligned}
$$

where θ_i represents the AoA of the ith incident signal, and $s_i(t)$ is the ith incident signal at the first antenna.

AoA Estimation with MUSIC
The basic idea of the standard MUSIC algorithm is eigenstructure analysis of an $M \times M$ correlation matrix $\mathbf{R_X}$ of received signal $\mathbf{X}$ at M antennas. From Equation 6, we express $\mathbf{R_X}$ as:

$$
\begin{aligned}
\mathbf{R_X} &= \mathbb{E}[\mathbf{XX}^\mathrm{H}] \\
&= \mathbf{A}\mathbb{E}[\mathbf{SS}^\mathrm{H}]\mathbf{A}^\mathrm{H} + \mathbb{E}[\mathbf{NN}^\mathrm{H}] \\
&= \mathbf{A}\mathbf{R_S}\mathbf{A}^\mathrm{H} + \sigma^2\mathbf{I} \qquad (7)
\end{aligned}
$$

where $\mathbf{R_S}$ is the correlation matrix of the complex signal vector. The correlation matrix $\mathbf{R_X}$ has M eigenvalues. The smallest $M-n$ eigenvalues are corresponding to the noise and the other n eigenvalues are corresponding to the n incident signals. The eigenvectors corresponding to the smallest $M-n$ eigenvalues construct a noise vector subspace $\mathbf{E_N} = [\mathbf{e}_1, \ldots, \mathbf{e}_{M-n}]$, and the other n eigenvectors construct a signal subspace $\mathbf{E_S} = [\mathbf{e}_{M-n+1}, \ldots, \mathbf{e}_M]$. The signal and the noise subspaces are orthogonal so the spatial spectrum function is expressed as:

$$P(\theta)_{MUSIC} = \frac{1}{\mathbf{a}^\mathrm{H}(\theta)\mathbf{E_N}\mathbf{E_N}^\mathrm{H}\mathbf{a}(\theta)} \qquad (8)$$

in which sharp peaks occur at the AoAs of the incident signals. In practice, we average multiple data samples to mitigate random noise and obtain the correlation matrix as below:

$$\widehat{\mathbf{R_X}} = \frac{1}{L}\sum_{i=1}^{L} \mathbf{XX}^\mathrm{H} \qquad (9)$$

where L is the number of samples employed.

Overview of Dynamic-MUSIC
To locate a human target with the reflected signal, our Dynamic-MUSIC method contains the following components:

- **Super-resolution AoA estimation:** With 3 antennas on the commodity Intel 5300 card, only two paths can be captured with the traditional MUSIC algorithm [29] and it also limits the resolution of AoA estimation. We leverage the fact that all static paths are merged into one on the spectrum due to signal coherence to significantly reduce the number of antennas required to capture all the paths. Moreover, the incoming signals also introduce phase differences across subcarriers besides across antennas. Based on this, we successfully obtain ToA estimation for each path and capture information in two dimensions.

- **Mobile paths identification:** Among all the reflection paths, we need to identify which paths are mobile paths reflected from the moving target. We observe that, when the human is walking, not always there is a reflection path from the target to the receiver. We employ this unique observation to identify the mobile paths. We take several AoA measurements within a short time window. The static path is always there. However, the mobile path may disappear due to the small movements of human target. By checking the stability of the path at slightly different locations, we can successfully identify the mobile paths at a high rate.

- **The target path identification:** Among the several mobile paths, we need to identify the one whose last reflector is the target. As described in previous session, the shortest mobile path is the target path, containing the angle information of the target. With the relative ToA for each path, we can identify the shortest mobile path and obtain its AoA.

- **Area coverage:** When the target is at some positions, the reflection path may not be detected. We propose a novel scheme to employ multiple consecutive measurements within a short time window to ensure the target path can be detected so the AoA can be obtained.

- **Target localization:** With the AoAs at multiple receivers, the location of the target can then be estimated.

Super-Resolution AoA Estimation
We leverage the 30 subcarriers available on the commodity Wi-Fi card to increase the number of effective sensors without any hardware modification, overcoming the 3-antenna barrier. Similar to SpotFi [19], the key insight is that incoming signals do not only introduce phase differences across antennas but also introduce phase differences across subcarriers. Different paths have different ToAs when reaching at the receiver. The time differences introduce measurable phase differences across subcarriers. For evenly-spaced subcarriers, the phase difference introduced across two adjacent subcarriers is $-2\pi f_\delta \tau$, where f_δ[1] is the subcarrier size and τ is the ToA. We denote the complex exponential of the introduced phase difference across subcarriers as a function of the ToA of the path:

$$\Omega(\tau_i) = e^{-j2\pi f_\delta \tau_i} \qquad (10)$$

where τ_i is the ToA of the ith propagation path. Based on this, we could form a virtual sensor array composed of all subcarriers. Thus, for M antennas and K subcarriers, we

---

[1] f_δ is 312.5 KHz for 40 MHz Wi-Fi channels.

obtain a total of $M \times K$ sensors. For a path with AoA θ and ToA τ, the steering vector in Equation 4 can be rewritten as:

$$\mathbf{a}(\theta, \tau) = [1, \ldots, \Omega_\tau^{K-1}, \ldots, \Phi_\theta^{M-1}, \ldots, \Phi_\theta^{M-1}\Omega_\tau^{K-1}]^\top \quad (11)$$

where Ω_τ and Φ_θ are abbreviations for $\Omega(\tau)$ and $\Phi(\theta)$. If the received signal of the ith path for the first subcarrier at the first antenna is $s_i(t)$, the received signal at each sensor is a superposition of all paths. When there are n signals arriving, the signal at the receiver in Equation 6 is rewritten as:

$$\mathbf{X}(t) = [\mathbf{a}(\theta_1, \tau_1), \ldots, \mathbf{a}(\theta_n, \tau_n)][s_1(t), \ldots, s_n(t)]^\top + \mathbf{N}(t) \quad (12)$$

The effective number of sensors $(M \times K)$ is now much larger than 3, breaking the number of antenna limit. Thus, the spectrum function in Equation 8 is rewritten as:

$$P(\theta, \tau)_{MUSIC} = \frac{1}{\mathbf{a}^{\mathrm{H}}(\theta, \tau)\mathbf{E_N}\mathbf{E_N}^{\mathrm{H}}\mathbf{a}(\theta, \tau)} \quad (13)$$

which is extended to provides both AoA and ToA estimations.

For traditional MUSIC algorithm, the coherence among signals degrades the performance significantly. Previous works [19, 47] remove the coherence by sacrificing the effective number of sensors and all multipath signals will be identified on the spectrum, shown in Figure 4(a). However, we find that we can utilize this 'bad' coherence to merge the useless paths so that the number of paths we need to detect is decreased without sacrificing any precious sensor. The key intuition is that without any spatial smoothing scheme to remove the coherence among signals, the static paths will merge together while the mobile paths will be clearly detected. We run benchmark experiments to verify this key finding. We let a person hold a steel plate so the steel plate generates a reflection path to the receiver. We carefully choose the position of the person to ensure the reflection path's AoA is at $45°$ for verification. If the person moves the plate slightly, the reflection path from the plate is a mobile path, otherwise it is a static path. We can clearly see in Figure 5(a), when the plate is static, we could only obtain one cluster of AoAs of the merged-static path and they do not change much. When the plate is moved, we obtain two clusters of AoAs in Figure 5(b): one belongs to the static path and the other belongs to the mobile path. The AoAs of the mobile paths are clustered at $45°$, matching the angle of the reflection path from the plate. So with a moving human, based on the signal vector in Equation 2, we can rewrite Equation 12 as:

$$
\begin{aligned}
\mathbf{X}(t) &= [\mathbf{a}(\theta_1, \tau_1), \ldots, \mathbf{a}(\theta_n, \tau_n)][s_1(t), \ldots, s_n(t)]^\top + \mathbf{N}(t) \\
&= \sum_{i=1}^{n_s} \alpha_i s_{s,1}\mathbf{a}_{s,i} + \sum_{i=1}^{n_m} s_{m,i}\mathbf{a}_{m,i} + \mathbf{N}(t) \\
&= [\sum_{i=1}^{n_s} \alpha_i \mathbf{a}_{s,i}, \mathbf{a}_{m,1}, \ldots, \mathbf{a}_{m,n_m}] \begin{bmatrix} s_{s,1} \\ s_{m,1} \\ \vdots \\ s_{m,n_m} \end{bmatrix} + \mathbf{N}(t) \quad (14)
\end{aligned}
$$

where $\mathbf{a}_{s,i}$ and $s_{s,i}$ are corresponding to the ith static path, and $\mathbf{a}_{m,i}$ and $s_{m,i}$ are corresponding to the ith mobile path.

Based on Equation 14, we can detect $n_m + 1$ paths [32]. All static paths we don't care about are merged into one path [47]

and we call it *merged-static path*. We purposely keep the coherence to merge all static paths to reduce the number of paths on the spectrum. The direct path signal is usually much stronger than the reflection path signals so the merged path peak is close to the original direct path peak on the spectrum shown in Figure 4(b). Thus, the useless static paths are merged and only one static path exists on the spectrum. On the other hand, the mobile-path signals and static path signals are incoherent and do not merge. When a mobile target is present, the mobile path signal which is important for us is detected together with the merged-static path shown in Figure 4(c).

Mobile Paths Identification
On the spectrum shown in Figure 4(c), mobile path and merged static path both exist. It's not easy to identify the mobile path on the spectrum without any environmental training. We observe that the merged-static path is detected all the time. However, when the human target is walking, not always a mobile path signal can be detected. We employ this unique observation to identify the mobile paths. We take several measurements within a short period of time. The merged-static path is always detected on the AoA spectrum. However, due to the small movements of human target, mobile paths may not be detected at some positions as shown in Figure 6(a). By checking the stability of the path on the spectrum at slightly different locations, we can successfully differentiate mobile paths with the merged-static path at a very high chance. With 20 measurements within 0.4 s, we can achieve a 98% identification rate as shown in Figure 6(b).

Identify the Target Path
If there are more than one mobile paths, we need to identify the mobile path which contains the target's location information. The shortest mobile path is the target path and we identify it by comparing the ToA of each mobile path. There are particular challenges to obtain the ToAs on commodity Wi-Fi cards.

First, nano-second level time synchronization between transmitter and receiver is difficult [25]. A sampling frequency offset (SFO) exists between a pair of transmitter and receiver for each packet transmission. Furthermore, there is a random packet detection delay (PDD) for each packet, which will introduce another additional time variance in the ToA estimation. Fortunately, the additional time introduced by SFO and PDD are the same for all the paths for one transmission so we can still employ the relative ToA to select the shortest one.

Unfortunately, the time delays introduced by SFO are different across two packet transmissions for the same transmitter-receiver pair. Meanwhile, the PDD is also random across packets. As we only obtain one CSI reading for one packet from commodity Wi-Fi cards, we need more than one packets to provide us multiple CSI readings for MUSIC algorithm. To include CSI from multiple packets for MUSIC processing, the relative ToAs need to be aligned to a same point.

The additional phase at the kth subcarrier is $-2\pi f_\delta(k - 1)\tau_{delay}$, where the τ_{delay} is the sum of time delays introduced by SFO (τ_{SFO}) and PDD (τ_{PDD}). The change is linear in frequency domain if the phase is not wrapped between 0 and 2π. Because all the RF chains on one Wi-Fi chipset are fully
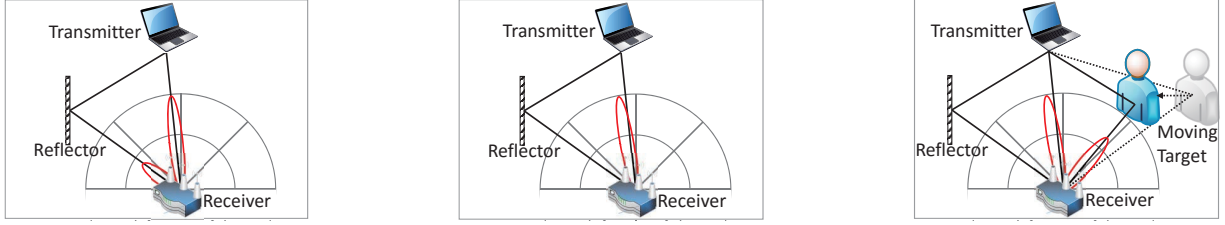
(a) Two static paths with spatial smoothing   (b) Two static paths with no spatial smoothing   (c) One merged-static path and a mobile path

Figure 4. **For clarity, we only show the AoA spectrum dimension. (a) With spatial smoothing to remove the coherence among signals, the two static paths are separated on the spectrum; (b) Without spatial smoothing, the two coherent static paths are 'merged' into one path on the spectrum; (c) The merged-static path and the mobile path are separated without spatial smoothing.**
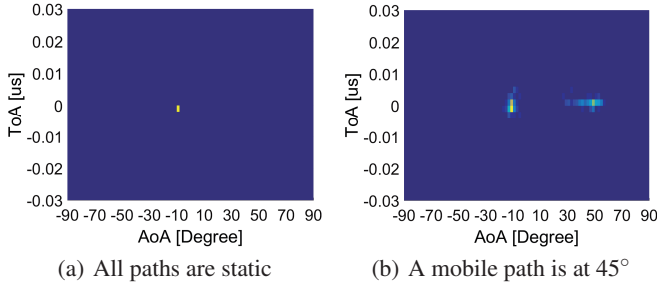
(a) All paths are static   (b) A mobile path is at $45°$

Figure 5. **Benchmark experiments: static paths are merged into one while static path and mobile path are separated**
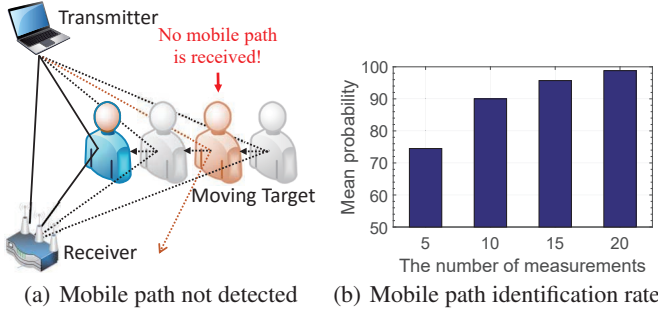
(a) Mobile path not detected   (b) Mobile path identification rate

Figure 6. (a) Mobile paths are not detected at some locations; (b) With multiple measurements to check the stability, the mobile path can be identified at a high rate.

synchronized, the additional phase introduced at a particular sub-carrier is the same for all antennas. We apply a linear fit method to remove this additional phase change and align all the relative ToAs across packets to the same point [31]. After the ToAs are aligned, the CSI from multiple packets can now be employed for the AoA and ToA estimations. Suppose $\varphi_i(m,k)$ is the unwrapped phase of the CSI at the kth subcarrier of the ith packet received at m^{th} antenna, we can obtain the optimal linear fit of the phase for the ith packet as:

$$\hat{\tau}_{delay,i} = \arg\min_{\xi} \sum_{m,k=1}^{M,K} (\varphi_i(m,k) + 2\pi f_\delta(k-1)\xi + \varepsilon)^2 \quad (15)$$

The $\hat{\tau}_{delay,i}$ includes the time delay of the ith packet and we can remove it to obtain the modified CSI phase as $\hat{\varphi}_i(m,k) = \varphi_i(m,k) + 2\pi f_\delta(k-1)\hat{\tau}_{delay,i}$. In this way, we subtract the random variance introduced by SFO and PDD for each packet

and obtain the CSI values with aligned relative ToAs across packets. For a single packet, this subtraction removes the same amount of time delay across all paths so identification of the shortest mobile path is not affected.

Area Coverage

Even when the target is not far away from the receiver, there may not be reflection path from the target to the receiver at some locations. However, one key observation is that, the target may not be detected at one location, it may be detected at a close-by location when the target moves just slightly. Based on this observation, we propose a novel scheme to take several consecutive measurements when the target is moving and combine the data to significantly increase the detection rate. In a very short time window, the position of a human target changes very little which will not affect the localization performance. If at least one measurement detects the target path in the time window, we can obtain the target path for localization. From our experiments, with only 3 measurements within 0.04 s, the target path detection rate is close to 100%. With this scheme, we can employ only two receivers to cover a relatively large monitoring area with a high detection rate. This sparse deployment property makes our method suitable for real-life large scale deployment.

Target Localization

Once we have the target's AoAs at multiple receivers, the target's location can be obtained. To remove the random angle variance and improve location accuracy, we employ the mean AoA value within a short time window for our location estimation. Although our system is able to locate the target with only two receivers, in general, the localization accuracy gets improved with more receivers. Suppose R receivers could be employed for localization in a monitoring area, the target position can then be estimated as:
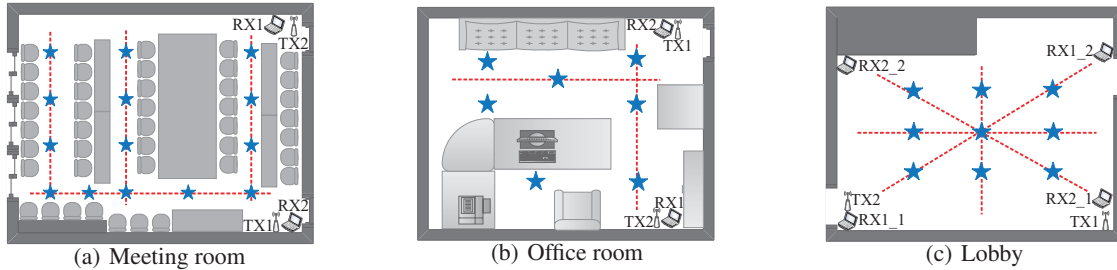
$$position = \arg\min_p \sum_{i=1}^{R} (\hat{\theta}_i - \theta_i)^2 \quad (16)$$

where $\hat{\theta}_i$ is the angle of position p to the ith receiver and θ_i is the estimated angle to the ith receiver.

EVALUATION

Implementation

We employ GIGABYTE miniPCs equipped with Intel 5300 Wi-Fi cards as the transmitters and receivers. 3 antennas are at-

Figure 7. Evaluation environments: (a) a meeting room of size $7 \, m \times 7.4 \, m$**; (b) an office room of size** $4.2 \, m \times 4.5 \, m$**; (c) a lobby area of size** $68.5 \, m^2$**. The blue pentagrams indicate the spots where the target spins and the red dotted lines are the walking routes.**

tached at each receiver. We install the CSI tool [11] developed by Halperin on these miniPCs to obtain the CSI information for each received packet. The CSI tool provides CSI information on 30 subcarriers. To reduce the amount of interference brought to the ongoing Wi-Fi transmissions in the building, our experiments are conducted in the 5 GHz frequency band employing an unused 40 MHz channel. Our system can be hosted on any channel in the 2.4 and 5 GHz bands with a suitable antenna array. The CSI values are estimated from the packet preamble part and our method has no requirement on the packet type. Our system can work with beacon packet, data packet or even dummy packet without a payload. Any transmission in the air can be employed for our location estimates and the system does not need to know the transmitters' locations. One intuitive solution is to employ the Wi-Fi beacon packets already exist in the air so no extra packets are needed to be transmitted. Therefore, our system has a minimum impact on the existing Wi-Fi data communications. We implement our system on a Dell M4800t laptop to process the CSIs from receivers and estimate the moving target's location.

We deploy our system in three typical indoor environments: an office room, a meeting room and a lobby. Figure 7 shows the floorplan of these three environments. In the office room and meeting room, there are a lot of furniture and electrical equipments so rich multipaths exist. We place the transmitter-receiver pairs as shown in Figure 7. In the office room and meeting room, we only deploy two receivers; in the lobby, we deploy upto 4 receivers to evaluate the effect of deployment densities. In each environment, we make the target spin slowly at randomly selected spots and walk at different speeds to evaluate the performance of our system. The human target walks along the trace at a constant speed each time. We use a video camera to record the whole process so the timestamp when the target is at a particular position can be easily retrieved to obtain the ground truth. We carefully measure the locations of the receivers when we deploy them.

Evaluation methodology: Because the human target is a polyhedron with a non-negligible size, it can't be treated as a point. For simplicity, we assume the human target has a width of 50 cm. As long as the target estimation is within this 50 cm range, we consider there is no localization error. Otherwise, we calculate the localization error as the minimum difference between the estimated location and this location range. Similarly, the angle estimation error is the minimum distance between the estimated angle and this angle range.

Localization Performance

Localization accuracy
As shown in Figure 8(a) and Figure 8(b), with only 2 receivers, we are able to achieve a median localization error of 40 cm for spinning and 36 cm for walking in the office room. In the meeting room, the median error increases slightly to 52 cm for spinning and 62 cm for walking. The main reason for slightly worse performance is the larger size of the meeting room with similar angle estimation accuracy. In the lobby, the median error is 60 cm and 62 cm respectively for spinning and walking. The lobby and the meeting room have similar sizes. Even though there are more objects in the meeting room with richer reflection paths, they have similar localization errors. This demonstrates that the static multipaths do not affect the system performance much.

Impact of different deployment strategies
As shown in Figure 7(c), if we only employ two receivers to locate the target, we have two different deployment strategies: the two receivers are placed at the corners of different sides (such as RX1_1-RX1_2 pair) or at the same side (such as RX1_1-RX2_2 pair). Figure 8(c) shows the CDF plot of localization error for the two deployment strategies. When we put the two receivers at different sides, the median localization error is 124 cm for spinning and 142 cm for walking. The localization errors are much higher than 60 cm for spinning and 62 cm for walking when the two receivers are placed at the same side. When receivers are placed at different sides, the two paths reflected from the target may have similar AoAs. Thus, their intersection point will be out of the monitoring area, deviating far from the ground truth. However, when receivers are at the same side, this issue is greatly mitigated. Note that, when there are more receivers, the performance difference between the two strategies decreases because the extra receivers will improve the overall performance.

Impact of deployment density of receivers
Although we could locate the moving target with only two receivers, a higher accuracy can be achieved with more receivers. We deploy 4 receivers in the lobby area and evaluate the impact of receiver density. Figure 9(a) shows the results: with 2 receivers, the median error is 60 cm for spinning and 62 cm for walking. With 3 receivers, the accuracy is improved to 46 cm for spinning and 50 cm for walking. With 4 receivers, the accuracy is further improved to 40 cm and 41cm respectively. So our system works well under sparse deployment
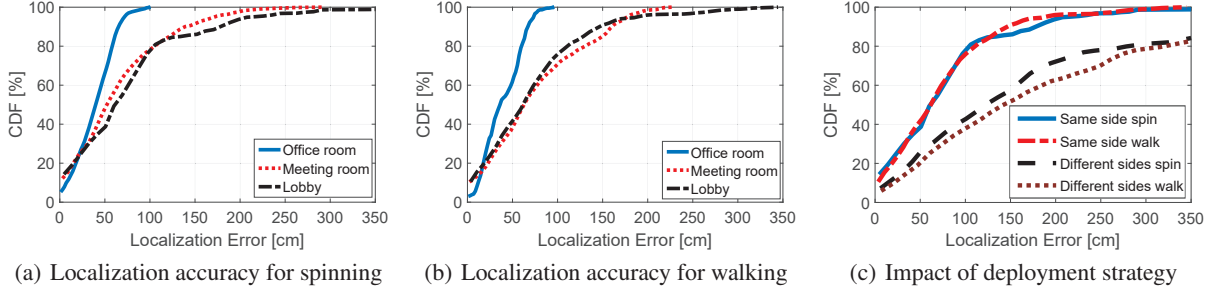
Figure 8. (a) Cumulative distribution function (CDF) plot of localization error in three different indoor environments for spinning; **(b)** CDF plot of localization error for walking; **(c)** CDF plot of localization error for different deployment strategies with only two receivers.

which makes it an ideal candidate for large scale deployment. More receivers can be employed for even better performance.

Impact of time window size
To remove the large random AoA variations, we average the AoA estimations in a time window. We vary the window size to evaluate its impact on localization performance. As shown in Figure 9(b), the best window size is 0.5 s and the median error is 60 cm for spinning and 62 cm for walking. If we locate the target without averaging, the error increases to around 1 m. When we employ a window size larger than 0.5 s, the target's movement will bring in AoA errors and the localization errors become larger again.

Impact of walking speed
We let the human target walk multiple times at different speeds to evaluate the effect in localization performance. The target walks at three different speeds: slow, normal and fast. The slow speed is between $0.5m/s$ to $1m/s$, the normal speed is between $1m/s$ to $1.5m/s$ and the fast speed is between $1.5m/s$ to $2m/s$. As shown in Figure 9(c), the median localization error is 61.2 cm for slow speed, 63.3 cm for normal speed and 61.4 cm for fast speed respectively. So the walking speed has little effect on the performance of our method.

Impact of number of samples
Based on Equation 9, we need to employ multiple samples to process the AoA. We vary the numbers of samples included in the Dynamic-MUSIC method to evaluate its effect. Figure 10(a) shows the CDF of localization error with different numbers of samples. With 10 samples, the median localization error is 192 cm. When we increase the number of samples, the error decreases to 71 cm for 20 samples and 80 cm for 40 samples. We achieve slightly better performance when we further increase the number of samples. With only 20 samples, our method has already achieved a good localization performance.

Angle estimation accuracy
Figure 10(b) shows the CDF of the target's angle estimation error. When the target is spinning, the median error is $4.6°$. When the target is walking, the median error increases slightly to $4.9°$. Note that the results are achieved with only 3 antennas. We also implement the traditional MUSIC algorithm for comparison. Limited by the number of antennas, traditional MUSIC algorithm is only able to capture two paths. The median error of angle estimation of the target is $9.6°$ for spinning and $9°$ for walking which are much larger compared to our

Dynamic-MUSIC method. The AoA resolution of our method is finer with ToA information from the second dimension. When two paths are too close in space domain to be separated, they may still be separated in time domain.

Sparse deployment coverage
The signal reflected from the human target is usually much weaker compared to the direct-path signal. What is worse, there may not be reflection path from the target to the receiver at some locations. We evaluate our scheme proposed in Section 4.6 in this section. We move the target's location while keep the distance between the target and the receiver unchanged. We test 100 target positions for each distance. We check whether the reflected signal from the target can be detected at the receiver. As shown in Figure 10(c), when the target is 9 m away from the receiver, our method can achieve a 69% detection rate with just one measurement. When the target distance to the receiver is deceased, the detection rate is higher. Then we take more than one measurements with an interval of 0.02 s. As shown in Figure 10(c), with two consecutive measurements, the probability of detecting the target path at least once is around 90%. With 3 measurements, the average detection rate is close to 100%. Also within a short 0.04 s interval, the target's location changes very little and does not affect the localization performance.

LIMITATIONS
Human target is not moving: Our Dynamic-MUSIC method works well with moving target. When the target is not moving, we have a low detection rate. However, even if the target is not moving, there are still subtle movements of the human body including breath. With a much larger bandwidth in 802.11ac and more antennas attached to the commodity AP, the resolution of our system can be improved significantly. We leave this challenging problem as our future work.

Multi-target localization: Passive multi-target localization is a well known challenging problem. Some previous works have proposed schemes to address this problem. However, these works either require dedicated hardware and special purpose signals [18, 55], or have a low accuracy in localization and the targets' quantity estimation [26, 27]. To handle this problem, we need to differentiate the mobile paths from different moving targets. The problem becomes even more difficult when several targets are near to each other. With a higher
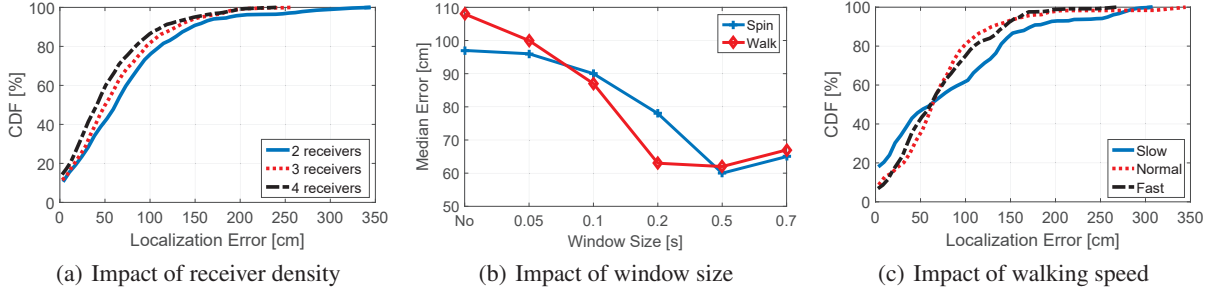
(a) Impact of receiver density   (b) Impact of window size   (c) Impact of walking speed

Figure 9. (a) CDF plot of localization error with different number of receivers; (b) median localization error with different window sizes; (c) CDF plot of localization error with different walking speeds.
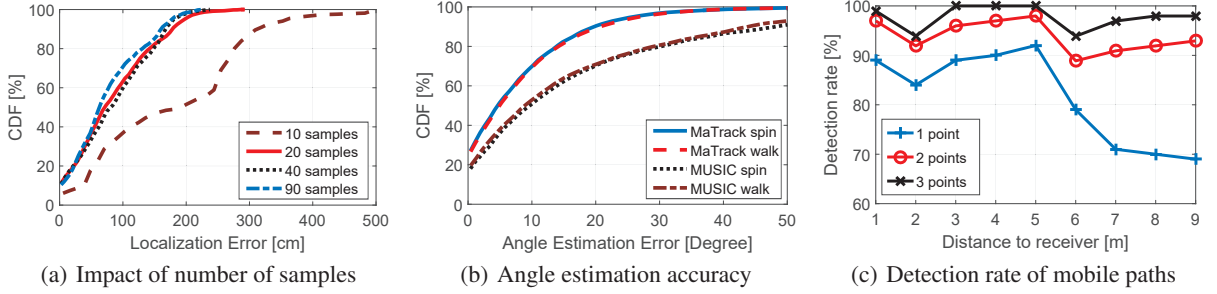

(a) Impact of number of samples   (b) Angle estimation accuracy   (c) Detection rate of mobile paths

Figure 10. (a) CDF plot of localization error with different numbers of samples; (b) CDF plot of target's angle estimation error; (c) detection rate of mobile paths with different numbers of measurements.

density deployment, we believe our method is able to locate sparsely-located multiple targets simultaneously.

Target path 100% blocked: The target path may be totally blocked at one receiver. However, it is not likely for multiple receivers to be blocked at the same time. In reality, we could deploy more receivers to ensure at least two receivers could capture the target path to mitigate the path blockage issue.

Automatic gain control: The AoA and ToA information are estimated purely from the phase information at the receiver side. So the automatic gain control and the transmission power do not affect the performance of our system.

CONCLUSION
We propose a novel Dynamic-MUSIC method that leverages the signal coherence, which is considered 'bad' in previous MUSIC-based localization systems to identify the moving target's AoA. Based on the proposed Dynamic-MUSIC method, we design and implement a device-free localization system on the commodity Wi-Fi cards without any offline training required. MaTrack is able to achieve below 0.6 m median error with only two receivers, each equipped with 3 antennas, outperforming the state-of-the-art methods.

SYMBOLS IN THIS PAPER
In order to make it easier to understand the math, Table 1 lists symbols used in this paper.

Symbol	Description
α	Constant difference between two signals
$\beta(t)$	Time-variant difference between two signals
$s(t)$	A path signal that is received at time t
$\mathbf{S}(t)$	Multipath signal vector at time t
$n/n_s/n_m$	The number of all/static/mobile path signals
θ	Angle-of-arrival of a path signal
τ	Time-of-arrival of a path signal
$\Phi(\theta)$	Adjacent antennas' phase difference
$\Omega(\tau)$	Adjacent subcarriers' phase difference
f_δ	Adjacent subcarriers' frequency difference
$\mathbf{a}(\theta)/\mathbf{a}(\theta,\tau)$	Steering vector of a path signal
$\mathbf{A}$	A matrix is composed of steering vectors
$x(t)$	Received signal on an antenna at time t
$\mathbf{X}(t)$	Received signal vector on an antenna array
$\mathbf{N}(t)$	Noise signal vector
$\mathbf{R}$	Correlation matrix of $\mathbf{X}(t)$
$\mathbf{I}$	Identity matrix
σ^2	Variance of $\mathbf{N}(t)$
M	The number of antennas
K	The number of subcarriers
$\mathbf{e}$	Eigenvector
$\mathbf{E}$	A subspace is composed of eigenvectors
$\varphi(m,k)$	The phase value of CSI of the kth subcarrier on the mth antenna

Table 1. Symbols are used in this paper

REFERENCES

1. Heba Abdel-Nasser, Reham Samir, Ibrahim Sabek, and Moustafa Youssef. 2013. MonoPHY: Mono-stream-based device-free WLAN localization via physical layer information. In *Proc. WCNC*. IEEE, 4546–4551.

2. Paramvir Bahl and Venkata N. Padmanabhan. 2000. RADAR: an in-building RF-based user location and tracking system. In *Proc. INFOCOM*, Vol. 2. IEEE, 775–784.

3. Q. Cai and J. K. Aggarwal. 1998. Automatic tracking of human motion in indoor scenes across multiple synchronized video streams. In *Proc. ICCV*. IEEE, 356–362.

4. Jose M. Chaquet, Enrique J. Carmona, and Antonio Fernández-Caballero. 2013. A survey of video datasets for human action and activity recognition. *Computer Vision and Image Understanding* 117, 6 (2013), 633 – 659.

5. Krishna Chintalapudi, Anand Padmanabha Iyer, and Venkata N. Padmanabhan. 2010. Indoor Localization Without the Pain. In *Proc. MobiCom*. ACM, 173–184.

6. N. Czink, M. Herdin, H. Özcelik, and E. Bonek. 2004. Number of multipath clusters in indoor MIMO propagation environments. *Electronics Letters* 40, 23 (Nov 2004), 1498–1499.

7. P. van Dorp and F. C. A. Groen. 2008. Feature-based human motion parameter estimation with radar. *IET Radar, Sonar Navigation* 2, 2 (April 2008), 135–145.

8. Hans Gellersen, Gerd Kortuem, Albrecht Schmidt, and Michael Beigl. 2004. Physical prototyping with Smart-Its. *IEEE Pervasive Computing* 3, 3 (July 2004), 74–82.

9. Sinan Gezici, Zhi Tian, Georgios B. Giannakis, Hisashi Kobayashi, Andreas F. Molisch, H. Vincent Poor, and Zafer Sahinoglu. 2005. Localization via ultra-wideband radios: a look at positioning aspects for future sensor networks. *IEEE Signal Processing Magazine* 22, 4 (July 2005), 70–84.

10. Mayank Goel, Chen Zhao, Ruth Vinisha, and Shwetak N. Patel. 2015. Tongue-in-Cheek: Using Wireless Signals to Enable Non-Intrusive and Flexible Facial Gestures Detection. In *Proc. CHI*. ACM, 255–258.

11. Daniel Halperin, Wenjun Hu, Anmol Sheth, and David Wetherall. 2011. Tool Release: Gathering 802.11N Traces with Channel State Information. *SIGCOMM Comput. Commun. Rev.* 41, 1 (Jan. 2011), 53–53.

12. Chunmei Han, Kaishun Wu, Y. Wang, and Lionel M. Ni. 2014. WiFall: Device-free fall detection by wireless networks. In *Proc. INFOCOM*. IEEE, 271–279.

13. Ju Han and Bir Bhanu. 2005. Human Activity Recognition in Thermal Infrared Imagery. In *Proc. CVPR Workshops*. IEEE, 17–17.

14. R. K. Harle and A. Hopper. 2005. Deploying and Evaluating a Location-aware System. In *Proc. MobiSys*. ACM, 219–232.

15. Pan Hu, Liqun Li, Chunyi Peng, Guobin Shen, and Feng Zhao. 2013. Pharos: Enable Physical Analytics Through Visible Light Based Indoor Localization. In *Proc. HotNets*. ACM, Article 5, 7 pages.

16. Seifallah Jardak, Sajid Ahmed, and Mohamed-Slim Alouini. 2014. Low complexity joint estimation of reflection coefficient, spatial location, and Doppler shift for MIMO-radar by exploiting 2D-FFT. In *Proc. International Radar Conference*. IEEE, 1–5.

17. Yifei Jiang, Xin Pan, Kun Li, Qin Lv, Robert P. Dick, Michael Hannigan, and Li Shang. 2012. ARIEL: Automatic Wi-fi Based Room Fingerprinting for Indoor Localization. In *Proc. Ubicomp*. ACM, 441–450.

18. Kiran Joshi, Dinesh Bharadia, Manikanta Kotaru, and Sachin Katti. 2015. WiDeo: Fine-grained Device-free Motion Tracing using RF Backscatter. In *Proc. NSDI*. USENIX, 189–204.

19. Manikanta Kotaru, Kiran Joshi, Dinesh Bharadia, and Sachin Katti. 2015. SpotFi: Decimeter Level Localization Using WiFi. In *Proc. SIGCOMM*. ACM, 269–282.

20. Ye-Sheng Kuo, Pat Pannuto, Ko-Jen Hsiao, and Prabal Dutta. 2014. Luxapose: Indoor Positioning with Mobile Phones and Visible Light. In *Proc. MobiCom*. ACM, 447–458.

21. Patrick Murphy, Ashu Sabharwal, and Behnaam Aazhang. 2006. Design of WARP: A wireless open-access research platform. In *Proc. Signal Processing Conference*. IEEE, 1–5.

22. Kazuya Ohara, Takuya Maekawa, Yasue Kishino, Yoshinari Shirai, and Futoshi Naya. 2015. Transferring Positioning Model for Device-free Passive Indoor Localization. In *Proc. UbiComp*. ACM, 885–896.

23. Qifan Pu, Sidhant Gupta, Shyamnath Gollakota, and Shwetak Patel. 2013. Whole-home Gesture Recognition Using Wireless Signals. In *Proc. MobiCom*. ACM, 27–38.

24. Tauhidur Rahman, Alexander T. Adams, Ruth Vinisha Ravichandran, Mi Zhang, Shwetak N. Patel, Julie A. Kientz, and Tanzeem Choudhury. 2015. DoppleSleep: A Contactless Unobtrusive Sleep Sensing System Using Short-range Doppler Radar. In *Proc. UbiComp*. ACM, 39–50.

25. Hariharan Rahul, Haitham Hassanieh, and Dina Katabi. 2010. SourceSync: A Distributed Wireless Architecture for Exploiting Sender Diversity. In *Proc. SIGCOMM*. ACM, 171–182.

26. Ibrahim Sabek and Moustafa Youssef. 2012. Multi-entity device-free WLAN localization. In *Proc. GLOBECOM*. IEEE, 2018–2023.

27. Ibrahim Sabek, Moustafa Youssef, and Athanasios V. Vasilakos. 2015. ACE: An Accurate and Efficient Multi-Entity Device-Free WLAN Localization System. *IEEE Trans. Mobile Computing* 14, 2 (Feb 2015), 261–273.

28. Ahmed Saeed, Ahmed E. Kosba, and Moustafa Youssef. 2014. Ichnaea: A Low-Overhead Robust WLAN Device-Free Passive Localization System. *IEEE Journal of Selected Topics in Signal Processing* 8, 1 (Feb 2014), 5–15.

29. Ralph O. Schmidt. 1986. Multiple emitter location and signal parameter estimation. *IEEE Trans. on Antennas and Propagation* 34, 3 (Mar 1986), 276–280.

30. Moustafa Seifeldin, Ahmed Saeed, Ahmed E. Kosba, Amr El-Keyi, and Moustafa Youssef. 2013. Nuzzer: A Large-Scale Device-Free Passive Localization System for Wireless Environments. *IEEE Trans. Mobile Computing* 12, 7 (July 2013), 1321–1334.

31. Souvik Sen, Božidar Radunović, Romit Roy Choudhury, and Tom Minka. 2012. You Are Facing the Mona Lisa: Spot Localization Using PHY Layer Information. In *Proc. MobiSys*. ACM, 183–196.

32. Tie-Jun Shan, Mati Wax, and Thomas Kailath. 1985. On spatial smoothing for direction-of-arrival estimation of coherent signals. *IEEE Trans. on Acoustics, Speech, and Signal Processing* 33, 4 (Aug 1985), 806–811.

33. Shuyu Shi, Stephan Sigg, and Yusheng Ji. 2013. Joint Localization and Activity Recognition from Ambient FM Broadcast Signals. In *Proc. UbiComp Adjunct*. ACM, 521–530.

34. Robert Steele, Amanda Lo, Chris Secombe, and Yuk Kuen Wong. 2009. Elderly persons' perception and acceptance of using wireless sensor networks to assist healthcare. *International journal of medical informatics* 78, 12 (2009), 788–801.

35. Hao Wang, Daqing Zhang, Yasha Wang, Junyi Ma, Yuxiang Wang, and Shengjie Li. 2016. RT-Fall: A Real-time and Contactless Fall Detection System with Commodity WiFi Devices. *IEEE Trans. Mobile Computing, In Press* (2016).

36. Jue Wang and Dina Katabi. 2013. Dude, Where's My Card?: RFID Positioning That Works with Multipath and Non-line of Sight. In *Proc. SIGCOMM*. ACM, 51–62.

37. Jue Wang, Deepak Vasisht, and Dina Katabi. 2014. RF-IDraw: Virtual Touch Screen in the Air Using RF Signals. In *Proc. SIGCOMM*. ACM, 235–246.

38. Pu Wang, Hongbin Li, and Braham Himed. 2011. Moving Target Detection Using Distributed MIMO Radar in Clutter With Nonhomogeneous Power. *IEEE Trans. on Signal Processing* 59, 10 (Oct 2011), 4809–4820.

39. Wei Wang, Alex X. Liu, Muhammad Shahzad, Kang Ling, and Sanglu Lu. 2015. Understanding and Modeling of WiFi Signal Based Human Activity Recognition. In *Proc. MobiCom*. ACM, 65–76.

40. Yan Wang, Jian Liu, Yingying Chen, Marco Gruteser, Jie Yang, and Hongbo Liu. 2014. E-eyes: Device-free Location-oriented Activity Identification Using Fine-grained WiFi Signatures. In *Proc. MobiCom*. ACM, 617–628.

41. Roy Want, Andy Hopper, Veronica Falcão, and Jonathan Gibbons. 1992. The Active Badge Location System. *ACM Trans. Inf. Syst.* 10, 1 (Jan. 1992), 91–102.

42. Joey Wilson and Neal Patwari. 2010. Radio Tomographic Imaging with Wireless Networks. *IEEE Trans. Mobile Computing* 9, 5 (2010), 621–632.

43. Rolf G. Winter, Aephraim M. Steinberg, and David Attwood. 2014. Coherence. In *AccessScience*. McGraw-Hill Education.

44. Kaishun Wu, Jiang Xiao, Youwen Yi, Min Gao, and Lionel M. Ni. 2012. FILA: Fine-grained indoor localization. In *Proc. INFOCOM*. IEEE, 2210–2218.

45. Jiang Xiao, Kaishun Wu, Youwen Yi, Lu Wang, and Lionel M. Ni. 2013. Pilot: Passive Device-Free Indoor Localization Using Channel State Information. In *Proc. ICDCS*. IEEE, 236–245.

46. Yaxiong Xie, Zhenjiang Li, and Mo Li. 2015. Precise Power Delay Profiling with Commodity WiFi. In *Proc. MobiCom*. ACM, 53–64.

47. Jie Xiong and Kyle Jamieson. 2013. ArrayTrack: A Fine-Grained Indoor Location System. In *Proc. NSIDI*. USENIX, 71–84.

48. Jie Xiong, Karthikeyan Sundaresan, and Kyle Jamieson. 2015. ToneTrack: Leveraging Frequency-Agile Radios for Time-Based Indoor Wireless Localization. In *Proc. MobiCom*. ACM, 537–549.

49. Han Xu, Zheng Yang, Zimu Zhou, Longfei Shangguan, Ke Yi, and Yunhao Liu. 2015. Enhancing Wifi-based Localization with Visual Clues. In *Proc. Ubicomp*. ACM, 963–974.

50. Lei Yang, Yekui Chen, Xiang-Yang Li, Chaowei Xiao, Mo Li, and Yunhao Liu. 2014. Tagoram: Real-time Tracking of Mobile RFID Tags to High Precision Using COTS Devices. In *Proc. MobiCom*. ACM, 237–248.

51. Zheng Yang, Zimu Zhou, and Yunhao Liu. 2013. From RSSI to CSI: Indoor Localization via Channel Response. *ACM Comput. Surv.* 46, 2, Article 25 (Dec. 2013), 25:1–25:32 pages.

52. Moustafa Youssef and Ashok Agrawala. 2005. The Horus WLAN Location Determination System. In *Proc. MobiSys*. ACM, 205–218.

53. Moustafa Youssef, Matthew Mah, and Ashok Agrawala. 2007. Challenges: Device-free Passive Localization for Wireless Environments. In *Proc. MobiCom*. ACM, 222–229.

54. Daqing Zhang, Hao Wang, Yasha Wang, and Junyi Ma. 2015. Anti-fall: A Non-intrusive and Real-Time Fall Detector Leveraging CSI from Commodity WiFi Devices. In *Proc. ICOST*. Springer, 181–193.

55. Wei Zhang, Wei Liu, Ju Wang, and Siliang Wu. 2013. DOA estimation of coherent targets in MIMO radar. In *Proc. ICASSP*. IEEE, 3929–3933.